Advances in Environmental Technology 1 (2019) 9-21

Advances in Environmental Technology

journal homepage: http://aet.irost.ir

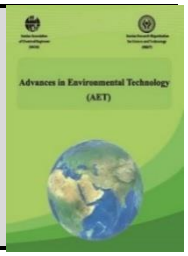

Fast and environmental-friendly degradation of *tert*-butyl mercaptan from contaminated soil using bimetallic-modified Fenton process

Pejman Roohi, Esmaeil Fatehifar*

Environmental Engineering Research Center (EERC), Faculty of Chemical Engineering, Sahand University of Technology, Sahand New Town, Tabriz, Iran

ARTICLE INFO

Article history:
Received 21 April 2019
Received in revised form
8 August 2019
Accepted 24 August 2019

Keywords:
Bimetallic
Modified Fenton
Remediation
tert-butyl mercaptan
Optimization

ABSTRACT

In this work, the fast remediation of *tert*-butyl mercaptan from the polluted soil via a bimetallic Fenton treatment that included $Fe^{2+}/Fe^{3+}/Fe^{0}/Cu^{2+}$ in the presence of gasoline was studied. The analysis of variance and the Pareto analysis resulting from the central composite design (CCD) showed that the H_2O_2, $CuSO_4$, Fe_3O_4 nanoparticles, nano zerovalent iron (nZVI), and gasoline initial concentrations as a secondary contaminant were influential factors on the removal efficiency of tert-butyl mercaptan (with an effectiveness of 2.09%, 13.38%, 1.92%, 2.01%, and 39.73% respectively). Moreover, the interaction of H_2O_2/nZVI, H_2O_2/nFe_3O_4, H_2O_2/$CuSO_4$, nZVI/nFe_3O_4, and nZVI/$CuSO_4$ had a positive effect on removal efficiency, while nFe_3O_4/$CuSO_4$ had a negative one. Surprisingly, the mixing of nZVI and nFe_3O_4 before adding them to the reactor did not affect the removal efficiency. The optimum conditions suggested for the maximum removal efficiency of tert-butyl mercaptan were the minimum levels of the initial gasoline concentration (2.5 %w/w), a maximum level of $CuSO_4$ (0.12 %w/w), and an optimum concentration of H_2O_2, nano-ZVI, and nano-Fe_3O_4 (8.92 %w/v, 0.1194 %w/w and 0.0898 %w/w, respectively) in the studied intervals. This condition led to a 99.27% efficiency removal of tert-butyl mercaptan removal in 20 minutes without pH and temperature adjustments.

1. Introduction

Tert-butyl mercaptan is widely used for various purposes such as natural gas odorization, the rubber industry, etc. The release of this odorant hydrocarbon has significant public safety health and environmental concerns. Exposure to *tert*-butyl mercaptan could lead to skin and eye irritation, other allergic reactions, muscular paralysis, dizziness, nausea, and central nervous system depression [1,2]. Furthermore, the secondary environmental impact of *tert*-butyl mercaptan (repulsive odor), including social dissatisfaction and economic problems due to the loss of tourist revenue, signify the importance of the remediation of this organosulfur. Over the last decades, a modified Fenton treatment has been developed for the remediation of soil and groundwater contaminated by a wide variety of hydrocarbons such as persistent organic pollutants (POPs) [3], polychlorinated biphenyls (PCBs) [4], nonaqueous-phase liquids (NAPLs) [5], polycyclic aromatic hydrocarbons (PAHs) [6] and gasoline [7]. In some studies, the Fenton treatment has been modified using iron nanoparticles to improve its removal efficiency with lower environmental impact [8-10]. The main reactions of the Fenton treatment process, which are based on the formation and consumption of hydroxyl radicals [11], are represented as follows [12]:

$$H_2O_2+Fe^{2+}\rightarrow Fe^{3+}+{}^{\bullet}OH+OH^{-} \quad (1)$$

$$Fe^{3+}+H_2O_2\rightarrow Fe^{2+}+{}^{\bullet}HO_2+H^{+} \quad (2)$$

$${}^{\bullet}OH+RH\rightarrow {}^{\bullet}R+H_2O \quad (3)$$

$${}^{\bullet}R+H_2O_2\rightarrow ROH+{}^{\bullet}OH \quad (4)$$

$${}^{\bullet}OH+Fe^{2+}\rightarrow Fe^{3+}+OH^{-} \quad (5)$$

$${}^{\bullet}OH+H_2O_2\rightarrow H_2O+{}^{\bullet}HO_2 \quad (6)$$

$${}^{\bullet}OH+{}^{\bullet}OH\rightarrow H_2O_2 \quad (7)$$

*Corresponding author. Tel: 0098-41-33459141
E-mail address: fatehifar@Sut.ac.ir
DOI: 10.22104/aet.2019.3561.1176

$Fe^{2+}+{}^{\bullet}HO_2 \rightarrow Fe^{3+}+ HO_2^-$ (8)

$Fe^{3+}+{}^{\bullet}HO_2 \rightarrow Fe^{2+}+O_2+2H^+$ (9)

${}^{\bullet}HO_2+H_2O_2 \rightarrow H_2O+{}^{\bullet}OH+O_2$ (10)

${}^{\bullet}HO_2+{}^{\bullet}HO_2 \rightarrow H_2O+O_2$ (11)

${}^{\bullet}O_2^- + Fe^{3+} \rightarrow Fe^{2+}+O_2$ (12)

$O^{\bullet}{}_2^- + Fe^{2+}+2H^+ \rightarrow Fe^{3+}+H_2O_2$ (13)

${}^{\bullet}HO_2+{}^{\bullet}O_2^-+H_2O \rightarrow H_2O_2+O_2+OH^-$ (14)

${}^{\bullet}OH+{}^{\bullet}HO_2 \rightarrow H_2O+O_2$ (15)

The mercaptan can be attacked with a hydroxyl radical to form disulfide and sulfonic acid. The overall reaction of mercaptan with hydrogen peroxide is represented in reactions 16 and 17 [13].

$2RSH+H_2O_2 \rightarrow RSSR+2H_2O$ (16)

$RSH+3H_2O_2 \rightarrow RSO_3H+3H_2O$ (17)

Over time, the modified Fenton treatment has been favored to obtain more efficient hydrocarbon removal [6,12,14,15]. In this method, hydrogen peroxide in a catalyzed system [16-18] with goethite [19], stabilizers and chelating agents [20,21], or magnetite [22-24] were used to remove some of the hydrocarbons. Moreover, various factors such as the pollutant aging and its physicochemical properties, organic matter of soil, reactant dosage, pH, soil texture, reaction time, and type of catalyst and stabilizers could affect the soil remediation efficiency [3,25]. There are a few studies concerning the remediation of *tert*-butyl mercaptan [26] via the Fenton modified process. Moreover, the removal of *tert*-butyl mercaptan from soil by a combination of a modified Fenton method with $KMnO_4$ and NaClO [27], sonication process [28], sono-Fenton process [29], and aerobic biodegradation [30] have been studied. These remediation processes investigate effective factors such as the initial oxidant concentration, iron ion concentration, sonication power, pollution load, etc. But so far, no one has investigated the impact of a bimetallic system such as copper/iron. Recently, nano-scale catalysts with enhanced reactivity have been widely applied to remediate contaminated soil [31-34]. Nanoparticles can pass through the porous media and remain suspended in aquifer systems due to their size. They have the potential capacity to be used for soil remediation. Magnetite nanoparticles (nFe_3O_4) have an inverse spinel structure with an FCC (face-centered cubic) unit cell. They contain both trivalent and divalent iron ions, where Fe^{3+} occupies both the tetrahedral and octahedral sites while Fe^{2+} occupies only the octahedral sites [22]. The use of nFe_3O_4 is a good alternative because it can be separated and reused to solve the recovery problem of the nanoparticles, as well as reducing remediation costs. Zero-valet iron (ZVI) is another catalyst which has been applied for a Fenton-like reaction. Recently, nano-scale zerovalent iron (nZVI) has been widely used to remediate contaminated soil and water [35-38]. Transition metals such as Ni(II) or Cu(II) and Co(II) can form complexes on the surface of solid iron in an aqueous Fenton system which can increase the reactivity of the iron nano-particles by producing reactive oxidants [39,40]. This modification leads to the formation of Fe ions that can be used for the oxidative removal of the pollutant. Since the electron affinity of Cu (1.235 eV) is greater than Ni (1.156 eV) [41,42], $CuSO_4$ is selected as an additive. Several studies used the Cu ion or bimetallic system in the Fenton treatment [43], but none of them used three types of iron ions, namely Fe^{2+}, Fe^{3+}, and Fe^0. The Fe-Cu bimetallic oxides, supported an aluminum-containing MCM-41 using 0.049 mol/L of H_2O_2 in Fenton system, 47% TOC reduction was achieved (pH=4, T=60 °C) [44]. Also, functional kaolin-supported bimetallic Fe/Ni nanoparticles (K-Fe/Ni) were applied for the removal of Direct Black G (DBG) [45]. In other work, a CuFe/SBA-15 bimetallic catalyst was utilized for the Fenton degradation of *N*, *N*-diethyl-*p*-phenyl diamine (DPD) with 83% destruction within 120 min [46]. Gong et al. used aerobic degradation of 4-chlorophenol (4-CP) over bismuth modified nZVI (Bi/Fe^0) due to the generation of a reactive oxygen species. In this method, the bismuth covering on the Fe^0 surface was under a zero-valent state [47]. Due to the social and environmental consequences of *tert*-butyl mercaptan and the little research concerning its remediation, this work aims to study the *tert*-butyl mercaptan oxidation yields in polluted soil via a modified Fenton process using bimetallic nano-particles of magnetite. In this work, the mass fraction of $CuSO_4$, Fe_3O_4 nanoparticles, and nZVI to the soil as well as the initial concentration of H_2O_2 with their positive, negative, and opposing effects were investigated. Central composite design (CCD) that was based on response surface methodology (RSM) was implemented to design the experiments. It led to the minimizing of the number of the experiments compared to the "one-factor-at-a-time"statistical approach [48] and analyzing of the effects of the factors and their interactions [49], mathematical modeling, and predict the optimal experimental condition [50-54]. To the best of our knowledge, enhanced remediation *of tert*-butyl mercaptan from polluted soil by use of $CuSO_4$, Fe_3O_4 nanoparticles, and nZVI in the Fenton treatment process has not been reported so far.

2. Materials and methods

2.1. Contaminated soil

Tabriz is located in Iran's East Azerbaijan province. It is a historical and tourist city with a population of more than 1.5 million. *Tert*-butyl mercaptan has been widely used for natural gas odorization in Tabriz. The characteristics of the sample soil collected from the industrial zone of this city are presented in Table 1. This soil was sampled from a 1-meter depth.

Table 1. Characteristics of the sample soil, collected from Tabriz zone

Characteristics	Value
Organic carbon (%)	1.3
Sand (%)	19.9
Silt (%)	57.7
Clay (%)	22.4
Crystalline Fe (mg/kg)	23240.0
Crystalline Mn (mg/kg)	419.0
Amorphous Fe (mg/kg)	53.2
Amorphous Mn (mg/kg)	28.8
pH	6.6

2.2. Chemical reactants and reactor

The reactants used for the tests and GC calibration were hydrogen peroxide (35% w/v) and *tert*-butyl mercaptan [55] (98% w/v), which were reagent grade from the Merck Company (Germany). Some of the physical and chemical properties of *tert*-butyl mercaptan are shown in Table 2. $CuSO_4$ (anhydrous, powder, ≥99.99% trace metals basis) and Fe_3O_4 nano powder (50-100 nm particle size, 97% trace metals basis and average surface area >60 m^2/g) were supplied by Sigma- Aldrich. The nZVI (average particles size of 50 nm, an average surface area of 20-25 m^2/g, a narrow particle size distribution of 20-100 nm and a high content of iron in the range of 80-90 %wt) was purchased from NANO IRON (Czech Republic). The deionized water was produced with a Pars Azma deionizer. All parts of the reactor were washed
with distilled water and sterilized at 110 °C for 50 min in order to eliminate all undesirable contaminants and microbial activity (the optimal temperature for microbial activity is 35 °C [56]). This sterilizing process was repeated five times. All experiments were performed in the batch reactor, which was made from 100 ml cylindrical glass (Figure 1). The polluted soil was agitated with a 20 rpm agitation system. The first and final concentration of the *tert*-butyl mercaptan in the soil system was monitored from five points around the reactor. These five points were averaged and recorded as the final result.

Table 2. Physical and chemical properties of *tert*-butyl mercaptan [55].

Hill Formula	Chemical Formula
$C_4H_{10}S$	$(CH_3)_3CSH$
Physical and chemical properties	
Molar Mass: 90.1872 g/mol	Colorless liquid, Stable and Flammable
Boiling point: 63.7-64.2 °C	**Solubility:** - Very soluble in alcohol, ether and liquid hydrogen sulfide - Slightly soluble in water ($2.0\times10^{+3}$ mg/L @ 25 °C (estimated))
Relative density (water = 1): 0.80	
Vapor density: 3.1 (Air= 1)	
Vapor Pressure: 181 mm Hg @ 25 °C (Extrapolated)	
Dissociation Constant: pKa = 11.22 @ 25 °C	

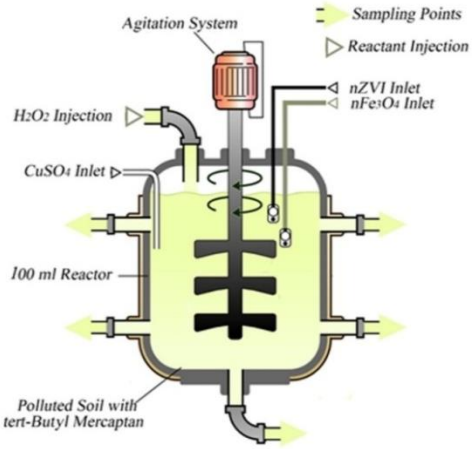

Fig. 1. Schematic of the experimental system used for bimetallic oxidation process

2.3. Material analyzing

Amorphous and crystalline iron and manganese oxyhydroxides were analyzed by citrate-bicarbonate-dithionite extractions [57]. For determining the organic carbon content, the sample soil was analyzed by combustion at 900 °C with the evolved CO_2 trapped in KOH and measured by the back titration of the unreacted OH^- [58]. The amount of the contaminant (*tert*-butyl mercaptan) in the polluted soil in parts per million by weight (ppm) were analyzed by a gas chromatograph (Agilent 7890) that was equipped with a flame ionization detector (FID), a thermal conductivity detector (TCD) , and an HP-Plot Q column. The fuel and carrier gas was H_2 (99.999%), the support gas was zero-grade dry air, and the make-up gas was He (99.999%) that were obtained from the Sabalan Company. The temperature program began at 105 °C for 2 min, ramped at 12 °C/min to 240 °C, and was held at 240 °C for 4 min with the column head gauge pressure of 3.9 psi. The injection port and detector temperatures were at 170 and 270 °C, respectively [27].

2.4. Procedure

A constant amount of soil (20 gr) was contaminated with gasoline, and *tert*-butyl mercaptan was added to the batch reactor. Next, the initial concentration of *tert*-butyl mercaptan was measured. Then, 5-level amounts of Fe_3O_4 nanoparticles (97% trace metal), nZVI (range of 80-90 %wt.), and $CuSO_4$ (99.99% trace metal) were added to the soil respectively. The polluted soil was oxidized with 20 ml of H_2O_2 and agitated for progress oxidation (20 min) with no temperature and pH adjustments. All experiments were conducted at the initial temperature of 24 °C and an initial pH of 6.6. Limited time interval resulted in a minimum influence of biodegradation, due to the slower reaction of the biodegradation process compared with chemical oxidation [30]. The removal efficiency of mercaptan contamination (%R) as a function of time is given by Eq. 18.

$$\text{Removal efficiency}(\%) = \frac{C_1 - C_2}{C_1} \times 100 \quad (18)$$

Where C_1 and C_2 are the initial *tert*-butyl mercaptan concentration (ppm) and its concentration after reaction time (ppm), respectively.

2.5. Design of experiments

In this study, a central composite design (CCD) based on the response surface method (RSM) was used to obtain the appropriate effects of the main factors and their interaction, which led to a mathematical model for the prediction of the remediation behavior. This method is an efficient way of determining the optimized condition [59]. The five factors under study included the initial concentrations of H_2O_2 (%w/v), Fe_3O_4 nanoparticles to soil ratio (%w/w), nZVI to soil ratio (%w/w), $CuSO_4$ to soil ratio (%w/w), and initial concentration of gasoline contaminant (%w/w). Their levels were determined by pre-experiment, safety, and legal considerations. The concentration ranges and levels of reactants are shown in Table 3.

Table 3. Experimental factors and their ranges and levels

Independent variables	Symbol	Factor Code	Ranges and levels				
			-2	-1	0	1	2
nZVI to soil ratio %(w/w)	$(nZVI:S)_0$	X_1	0.04	0.06	0.08	0.10	0.12
Initial H_2O_2 concentration %(w/v)	$[H_2O_2]_0$	X_2	1	3	5	7	9
$CuSO_4$ to soil ratio %(w/w)	$(CuSO_4:S)_0$	X_3	0.04	0.06	0.08	0.10	0.12
Initial gasoline to soil ratio %(w/w)	$(I.C:S)_0$	X_4	2.5	5	7.5	10	12.5
nFe_3O_4 to soil ratio %(w/w)	$(nFe_3O_4:S)_0$	X_5	0.03	0.05	0.07	0.09	0.11

Table 4.The 5-factors 5-level CCD matrix with the observed and the predicted responses.

Standard order	Run order	Block	Coded values					Removal efficiency (%)	
			$(nZVI:S)_0$	$[H_2O_2]_0$	$(CuSO_4:S)_0$	$(I.C:S)_0$	$(nFe_3O_4:S)_0$	Observed	Predicted
4	1	1	1.00	1.00	-1.00	-1.00	1.00	78.700	78.514
9	2	1	-1.00	-1.00	-1.00	1.00	-1.00	69.480	68.604
20	3	1	0.00	0.00	0.00	0.00	0.00	74.910	74.990
12	4	1	1.00	1.00	-1.00	1.00	-1.00	64.456	64.059
6	5	1	1.00	-1.00	1.00	-1.00	1.00	78.700	78.523
18	6	1	0.00	0.00	0.00	0.00	0.00	75.180	74.990
13	7	1	-1.00	-1.00	1.00	1.00	1.00	64.210	63.518
14	8	1	1.00	-1.00	1.00	1.00	-1.00	71.040	70.652
2	9	1	1.00	-1.00	-1.00	-1.00	-1.00	69.155	68.783
16	10	1	1.00	1.00	1.00	1.00	1.00	77.251	77.049
5	11	1	-1.00	-1.00	1.00	-1.00	-1.00	80.150	79.363
7	12	1	-1.00	1.00	1.00	-1.00	1.00	76.510	75.898
10	13	1	1.00	-1.00	-1.00	1.00	1.00	69.360	69.094
1	14	1	-1.00	-1.00	-1.00	-1.00	1.00	77.670	76.994
21	15	1	0.00	0.00	0.00	0.00	0.00	73.910	74.990
22	16	1	0.00	0.00	0.00	0.00	0.00	76.080	74.990
11	17	1	-1.00	1.00	-1.00	1.00	1.00	69.450	68.748
17	18	1	0.00	0.00	0.00	0.00	0.00	74.147	74.990
15	19	1	-1.00	1.00	1.00	1.00	-1.00	72.620	71.808
19	20	1	0.00	0.00	0.00	0.00	0.00	76.560	74.990
3	21	1	-1.00	1.00	-1.00	-1.00	-1.00	71.510	70.714
8	22	1	1.00	1.00	1.00	-1.00	-1.00	82.130	81.822
31	23	2	0.00	0.00	0.00	0.00	-2.00	68.505	69.269
30	24	2	0.00	0.00	0.00	2.00	0.00	69.130	69.693
27	25	2	0.00	0.00	-2.00	0.00	0.00	70.570	70.597
32	26	2	0.00	0.00	0.00	0.00	2.00	72.250	72.402
29	27	2	0.00	0.00	0.00	-2.00	0.00	83.610	83.962
23	28	2	-2.00	0.00	0.00	0.00	0.00	68.460	69.832
26	29	2	0.00	2.00	0.00	0.00	0.00	73.420	73.823
33	30	2	0.00	0.00	0.00	0.00	0.00	76.025	74.990
25	31	2	0.00	-2.00	0.00	0.00	0.00	70.040	70.552
28	32	2	0.00	0.00	2.00	0.00	0.00	79.000	78.879
24	33	2	2.00	0.00	0.00	0.00	0.00	73.501	73.044

A blocking technique was used for investigating the reactant addition mode. In mode 1, nZVI and nFe_3O_4 were mixed together and then added to the contaminated soil. In mode 2, nZVI and nFe_3O_4 were poured into the reactor separately. Moreover, a randomization technique was used to guard against unknown and uncontrolled factors as lurking

nuisance factors. The coded variables resulting from Eq. 19 were used for statistical calculations for simplicity in the experimental design as follows:

$$x_i = \frac{X_i - X_c}{\delta X} \quad (19)$$

where x_i, δX, X_i, and X_c are the coded value of the independent variables, the step change, the actual values of the independent variables, and the actual values of the independent variables at the center point, respectively.

3. Results and discussion

3.1. CCD method

The design of the experiment via CCD in the 5-factor 5-level matrix is summarized in Table 4. In this study, 33 experiments were performed: 16 cubic points, 7 replicates at the center point in cubes and axial (α = 0), and 10 axial points (α = ±2). Blocks 1 and 2 represent the experiments which were conducted in nZVI and nFe_3O_4 addition mode 1 and 2, respectively.

For the prediction of the response, a quadratic polynomial response was used as Eq. 20:

$$Y = \beta_0 + \sum_{i=1}^{k} \beta_i x_i + \sum_{i=1}^{k} \beta_{ii} x_i^2 + \sum_{i=1}^{k-1} \sum_{j=2}^{k} \beta_{ij} x_i x_j + \epsilon \quad i \neq j \quad (20)$$

Where, Y, x_i and x_j, $x_i x_j$ and ε are the response variable, coded independent variables, coded interaction term and random error accounting for the differences between observed and predicted results, respectively. β_0, β_i, β_{ii} and β_{ij} are intercepting term, linear, quadratic and interaction effects in the prediction model, respectively. i and j represent the index numbers for the patterns, in which $i<j$ must be observed for the interaction term.k denotes the number of input variables [60,61]. According to the results of the experiments and those of Eq. 20, to predict the response concerning the main factors and their interactions, an experimental mathematical model was obtained in coded values (Eq. 21).

$$Y=74.4903+0.8031\times x_1+0.8176\times x_2+2.0704\times x_3-3.5674\times x_4+0.7833\times x_5-0.8881\times x_1^2-0.7007\times x_2^2-0.0631\times x_3^2+0.4593\times x_4^2-1.0388\times x_5^2+0.9814\times x_1x_2+1.3794\times x_1x_3+0.2189\times x_1x_4+1.4496\times x_1x_5+0.9975\times x_2x_3+0.4070\times x_2x_4+0.6925\times x_2x_5-0.5050\times x_3x_4-1.8655\times x_3x_5-0.3725\times x_4x_5 \quad (21)$$

3.2. Analysis of variance (ANOVA)

Based on the results from Table 4, the analysis of variance (ANOVA) is summarized in Table 5. Because the significance level (α) is 0.05 for a certain degree of freedom (DF), if the *P*-value for each factor is smaller than 0.05, it is recognized as an effective factor [62-64].

According to Table 5, the iron catalysts addition mode (catalysts mixing before/after addition to soil) is not an effective factor in the studied interval because the *P*-value is greater than 0.05 for the blocks (*P*-value=0.103). Also, the *P*-value of the lack-of-fit (0.617) indicates that variations in the data around the mathematical model (Eq. 21) are not significant relative to the pure error and adequately fits the data with the high correlation coefficient (R^2=0.9851) [65; 66]. Moreover, the *P*-values show that the linear, square and interactions are significant on the variation in the removal efficiency of *tert*-butyl mercaptan (*P*-values<0.05). Table 6 shows the *P* and t values for the estimated regression coefficients. This table indicates that the five main factors and the interactions effect of H_2O_2/nZVI, H_2O_2/nFe_3O_4, H_2O_2/ $CuSO_4$, nZVI/$CuSO_4$, nZVI/nFe_3O_4, and $CuSO_4$/nFe_3O_4 are significant in the model.

Table 5. ANOVA table for *tert*-butyl mercaptan removal from soil.

	DF	SS	MS	F-	P-value
Blocks	1	3.037	3.037	3.150	0.103
Regression	20	698.819	34.941	36.28	0.000
Linear	5	454.563	90.913	94.40	0.000
Square	5	75.917	15.183	15.29	0.002
Interaction	10	168.339	16.834	17.48	0.000
Residual	11	10.594	0.963		
Lack-of-Fit	6	5.141	0.857	0.79	0.617
Pure error	5	5.453	1.091		
Total	32	712.450			
R^2=98.51%					

Table 6. Estimated regression coefficients, t-values and *P*-values.

Terms	Terms removal of *tert*-butyl mercaptan		
	Coefficient	t-Value	P-value
β_0	74.9903	203.471	0.000
β_1	0.8031	4.009	0.002
β_2	0.8176	4.081	0.002
β_3	2.0704	10.336	0.000
β_4	-3.5674	-17.809	0.000
β_5	0.7833	3.910	0.002
β_{11}	-0.8881	-4.975	0.000
β_{22}	-0.7007	-3.925	0.002
β_{33}	0.0631	0.353	0.731
β_{44}	0.4593	2.573	0.026
β_{55}	-1.0388	-5.820	0.000
β_{12}	0.9814	4.000	0.002
β_{13}	1.3794	5.622	0.000
β_{14}	0.2189	0.892	0.391
β_{15}	1.4469	5.897	0.000
β_{23}	0.9975	4.066	0.002
β_{24}	0.4070	1.659	0.125
β_{25}	0.6925	2.823	0.017
β_{34}	-0.5050	-2.058	0.064
β_{35}	-1.8655	-7.604	0.000
β_{45}	-0.3725	-1.518	0.157

The Pareto analysis resulting from Eq. 22 demonstrates the comparison between the influence of the main factors and the interactions [67].

$$P_i = \left(\frac{\beta_i^2}{\sum \beta_i^2}\right) \times 100 \qquad i \neq 0 \tag{22}$$

The Pareto graph analysis represents the percentage effect of each factor on the response (Figure 2). In order to obtain a simpler empirical model and a better fit for the removal efficiency, the insignificant terms can be removed from Eq. 19, which then represents the final model in coded form (Eq. 23).

$$Y=74.4903+0.8031\times x_1+0.8176\times x_2+2.0704\times x_3-3.5674\times x_4+0.7833\times x_5-0.8881\times x_1^2-0.7007\times x_2^2+0.4593\times x_4^2-1.0388\times x_5^2+0.9814\times x_1x_2+1.3794\times x_1x_3+1.4496\times x_1x_5+0.9975\times x_2x_3+0.6925\times x_2x_5-1.8655\times x_3x_5 \tag{23}$$

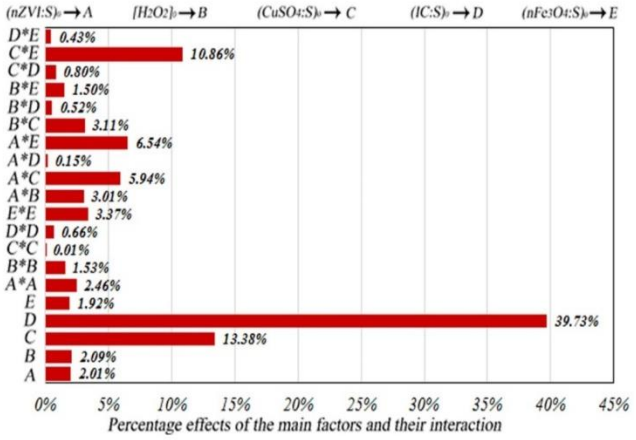

Fig.2. Pareto graphic analysis of the main factors and interactions.

3.3. Effects of the main factors and interactions

The effects of the operational parameters on the removal efficiency of the *tert*-butyl mercaptan by the modified Fenton treatment are shown in Figure 3. As demonstrated in Figure 3(a), the removal efficiency of the *tert*-butyl mercaptan from polluted soil increases as the nZVI to soil ratio increases in constant amounts of the other main parameters ($[H_2O_2]_0$=5% %w/v, $(CuSO_4{:}S)_0$=0.08 %w/w, $(IC{:}S)_0$=7.5 %w/w, $(nFe_3O_4{:}S)_0$=0.07 %w/w). This figure shows that increasing the nZVI up to a certain level leads to higher *tert*-butyl mercaptan removal efficiency. But the removal efficiency decreases with any further addition of nZVI due to the side and propagation reactions (Eqs. 5, 8 and 13).

Figure 3(b) shows that the addition of $CuSO_4$ to the reaction increased the removal efficiency. With respect to reaction 24, the Fe(II) generated by the oxidation of the nZVI surface with H_2O_2 is limited and is not enough to fully consume the H_2O_2. Due to this phenomenon, hydroxyl radicals generated in the catalytic system (reaction 1) is low, and a cation needs to be added to enhance the reactivity of nZVI in the Fenton system by producing more •OH.

$$H_2O_2+Fe^0(s) \rightarrow 2H_2O+Fe^{2+}(s) \tag{24}$$

Adding Cu(II) to induce better conditions for the supply of Fe(II) from nZVI (reaction 25), leads to a better remediation yield.

$$Cu^{2+}+Fe^0(s) \rightarrow Cu_0+Fe^{2+}(s) \tag{25}$$

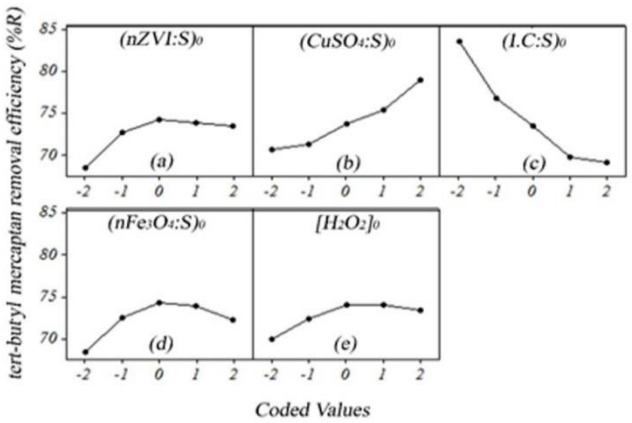

Fig. 3. (a) The effect of nZVI to soil ratio (%w/w), (b) The effect of $CuSO_4$ to soil ratio (%w/w), (c) The effect of initial *tert*-butyl mercaptan to soil ratio (%w/w) (d) The effect of Fe_3O_4 to soil ratio (%w/w) and (e) The effect of initial H_2O_2 concentration (%w/v) on *tert*-butyl mercaptan removal efficiency. T_0=24 °C, pH_0=6.6, Time=20 min.

As the $CuSO_4$ participates in the reactions, the Cu^{2+} enhances the nZVI reactivity, but the SO_4^{2-} can block the reactive sites of Fe^0 by the formation of inner-sphere complex-forming ligands [6,8] (reaction 24) that consume Fe^{2+} and Fe^{3+} and can reduce the removal efficiency. Therefore, $CuSO_4$ participation leads to two opposite results because of Cu^{2+} and SO_4^{2-}. As illustrated in Figure 3(b), increasing $CuSO_4$ concentration increases the removal efficiency. Therefore, the positive effect of Cu^{2+} from reaction 25 and H_2O_2-$CuSO_4$ has a higher removal efficiency when compared with that of reaction 26.

$$Fe^{2+}+Fe^{3+}+SO_4^{2-}+12H_2O \rightarrow Fe_6(OH)_{12}SO_4+12H^+ \tag{26}$$

When the initial gasoline concentration increases, the pollutant is more exposed to the oxidizing agent due to the solubility of mercaptan to gasoline. On the other hand, some possible zones of accumulated contaminant are created, which hinders the contact between the target organic pollutants, and this led to less accessibility for oxidation remediation. Furthermore, some of the oxidation agent molecules attack to degrade the gasoline. These two phenomena will lead to two competing results. As demonstrated in Figure 3(c), when the initial gasoline concentration increases, the removal efficiency falls, but its slope decreases.As demonstrated in Figure 3(d), the *tert*-butyl mercaptan removal efficiency increases as the Fe_3O_4 nanoparticles are raised up to a certain level (about 0.09 %w/w) in constant amounts of the other main parameters ($[H_2O_2]_0$=5% %w/v, $(nZVI{:}S)_0$=0.08 %w/w, $(CuSO_4{:}S)_0$=0.08 %w/w, $(IC{:}S)_0$=7.5 %w/w). But the removal efficiency falls with the further addition of nFe_3O_4 due to the side and propagation reactions (Eqs. 5, 8 and 13). Figure 3(e)

illustrates the effect of the initial H_2O_2 concentration on *tert*-butyl mercaptan removal efficiency (%R). This figure shows that the removal efficiency increases with the initial hydrogen peroxide concentration up to a certain level (about 7 %w/v). Further increasing of H_2O_2 concentration leads to a decrease in *tert*-butyl mercaptan degradation efficiency. According to reactions 6, 7 and 15 [67; 69; 70] this result is due to a series of propagation reactions and scavenging that produce less reactive radicals such as hydroperoxide radicals and hydroxyl ions ($^{\bullet}OOH$ and OH^-). According to Table 6 and the mathematical model (Eq. 21), the interaction between the initial H_2O_2 concentration and nZVI to soil ratio is an effective factor on the removal efficiency. Fe^{2+} is an alternative to enable more extensive and greater contaminant oxidation. As represented in Figure 4, increasing the hydrogen peroxide concentration or nZVI to a certain level could increase the removal efficiency due to $^{\bullet}OH$ radicals generation [67,71-73]. A higher concentration of H_2O_2 or nZVI decreases the removal efficiency due to a series of side and propagation reactions like Equations 5, 6, 7, 8 and 15 [67,69,70].

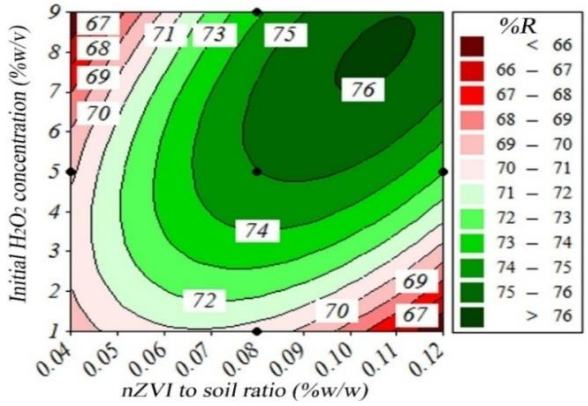

Fig. 4. Counter plot of *tert*-butyl mercaptan removal efficiency as a function of interaction between H_2O_2 and nZVI in constant amounts of the other main parameters ($[H_2O_2]_0$=5% %w/v, $(nZVI:S)_0$=0.08 %w/w, $(CuSO_4:S)_0$=0.08 %w/w, $(IC:S)_0$=7.5 %w/w). T_0=24 °C, pH_0=6.6, Time=20 min.

Figure 5 illustrates that nZVI and nFe_3O_4 have an effective interaction which increases *tert*-butyl mercaptan removal efficiency. In a low concentration of nZVI, the removal efficiency falls due to the side reaction, which is illustrated before. This result is similar to nFe_3O_4. But when nZVI and nFe_3O_4 are used in the reaction, the Fe_3O_4 nanoparticles would restrain the formation of a passivated layer on the nZVI surface [74]. As a result, the nFe_3O_4 made a medium to promote the electron transfer between the nZVI and *tert*-butyl mercaptan. Because of the electron transfer from Fe^0 to magnetite Fe(III) (Eq. (27)) and the $^{\bullet}OH$ formation in Fe_0/iron oxide suspensions, the Fe_3O_4/Fe^0 possessed a higher activity than the pure Fe_3O_4 or Fe^0.

$$Fe^0+2Fe(II)\rightarrow 3Fe(III) \quad (27)$$

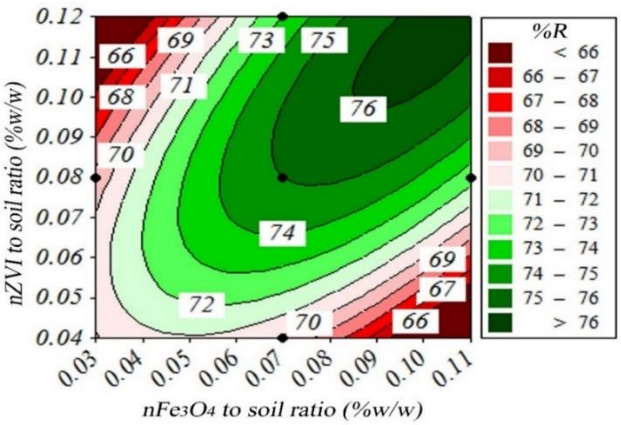

Fig. 5. Counter plot of *tert*-butyl mercaptan removal efficiency as a function of interaction between nZVI and nFe_3O_4 with constant amounts of the other main parameters at the center point, T_0=24 °C, pH_0=6.6, Time=20 min.

Figure 6 and Table 6 show that the H_2O_2 and nFe_3O_4 interaction has a positive role on removal efficiency. As shown in reactions 2, 9 and 12, Fe^{3+} is an alternative to enable fast and could promote a reaction by reactive radical generation for contaminant oxidation. In these reactions, Fe^{3+} is consumed while Fe^{2+} is generated. From the reactions 1 and 2, which, $^{\bullet}OH$ is generated from H_2O_2/Fe^{2+} while $^{\bullet}OH_2$ is generated from H_2O_2/Fe^{3+}. Therefore, Fe^{2+} generation leads to higher *tert*-butyl mercaptan removal efficiency due to higher reactivity of OH compared with $^{\bullet}OH_2$. Figure 6 demonstrates that with low H_2O_2 concentration, an increase in nFe_3O_4 in the studied interval decreases the removal efficiency. This phenomenon is due to the side reaction that results from the excess Fe^{2+} that is not fully consumed by the H_2O_2. As the H_2O_2 concentration is raised up to a certain level, the *tert*-butyl mercaptan removal efficiency increases and the Fe^{2+} is fully used for the oxidation reaction.

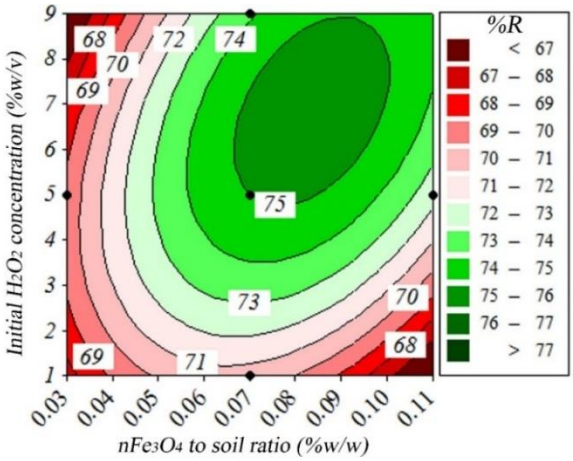

Fig.6. Counter plot of *tert*-butyl mercaptan removal efficiency as a function of interaction between H_2O_2 and nFe_3O_4 with constant amounts of the other main parameters at the center point, T_0=24 °C, pH_0=6.6, Time=20 min.

As represented in Figure 7 and Table 6, the H_2O_2 and $CuSO_4$ interaction has a positive role in removal efficiency. As

shown in reactions 28 and 29, the Cu^{2+} can promote a reaction by reactive radical generation (•OH and $•HO_2$) for contaminant oxidation. This figure and Equation 23 shows that Cu^{2+} affect, as a catalyst, are more than nFe_3O_4 and nZVI in the presence of H_2O_2 ($H_2O_2/CuSO_4$ > H_2O_2/nZVI> H_2O_2/nFe_3O_4).

$$Cu^{2+} + H_2O_2 \rightarrow Cu^{+} + •HO_2 + H^{+} \quad (28)$$

$$Cu^{+} + H_2O_2 \rightarrow Cu^{2+} + •OH + OH^{-} \quad (29)$$

Figure 7 demonstrates that when the H_2O_2 concentration was raised to a certain level, there was an increase in *tert*-butyl mercaptan removal efficiency. The maximum *tert*-butyl mercaptan removal efficiency was achieved in the maximum initial Cu^{2+} concentration in the studied interval.

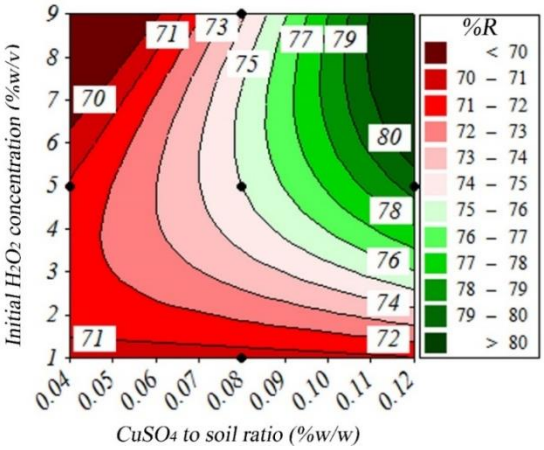

Fig. 7. Counter plot of *tert*-butyl mercaptan removal efficiency as a function of interaction between H_2O_2 and $CuSO_4$ with constant amounts of the other main parameters at the center point, T_0=24 °C, pH_0=6.6, Time=20 min.

As shown in Figure 8 and Table 6, the interaction between nZVI and $CuSO_4$ plays a positive role in the *tert*-butyl mercaptan remediation process. The oxidation-reduction mechanism which can be suggested for Cu^{2+} and nZVI interaction is justified by the difference in Cu^{2+}/Cu^0 and Fe^{2+}/Fe^0 standard potentials. A comparison between the standard redox potential of Cu^{2+}/Cu^0 and Fe^{2+}/Fe^0 indicate that Cu(II) can be reduced to Cu^0 because of electron transfer from the nZVI surface and oxidized iron ($E0_{Cu^{2+}/Cu(s)}$=+0.34 V > $E0_{Fe^{2+}/Fe(s)}$=−0.44 V at 298 K) [75]. Therefore, Cu(II) leads to the release of Fe^{2+} (reaction 25) from the nZVI surface, which is essential for the reaction with H_2O_2 to produce a higher content of •OH to enhance the removal efficiency.

Table 6 illustrates the effect of the $CuSO_4$ and nFe_3O_4 interaction on removal efficiency. Surprisingly, Figure 9 shows that the $CuSO_4$ concentration increases the *tert*-butyl mercaptan removal efficiency in the presence of the minimum nFe_3O_4 concentration while the maximum nFe_3O_4 level in the studied intervals decreased it. These phenomena could be a result of Cu(II) reduction [76,77] and Fe(II) oxidized to Fe(II) (reactions 30 and 31 [78,79]). In reaction 30, Fe(II) was consumed, and Fe(III) was produced. As a result, reactions 1, 2, 9 and 12 showed that the Fe(III) reactions compared with the Fe(II) ones generated less reactive species, which led to lower *tert*-butyl mercaptan removal efficiency [80,81]. In reaction 1 with Fe(II), •OH was produced, while $•HO_2$ and O_2 were produced by the reaction of Fe(III) (reactions 2, 9 and 12), which were lower reduction potential compared with •OH [82]. In reaction 31, Cu(II) was reproduced, and $•HO_2$ was consumed in reactions 8, 9, 10, 11, 14 and 15. Moreover, SO_4^{2-} consumed Fe^{2+} and Fe^{3+} due to reaction 26 and could reduce the removal efficiency.

$$Cu(II)_{aq} + Fe(II)_{aq} \leftrightarrow Cu(I)_{aq} + Fe(III)_{aq} \quad (30)$$

$$Cu(I)_{aq} + O_2 \leftrightarrow Cu(II)_{aq} + •HO_2 \quad (31)$$

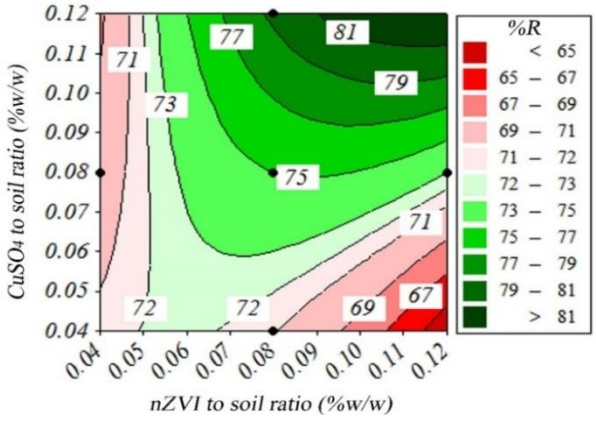

Fig. 8. Counter plot of *tert*-butyl mercaptan removal efficiency as a function of interaction between nZVI and $CuSO_4$ with constant amounts of the other main parameters at the center point, T_0=24 °C, pH_0=6.6, Time=20 min.

The results of the experiments showed that the presence of Cu(II) had two opposite effects on removal efficiency. On the one hand, the positive role of the interaction of Cu^{2+}/nZVI and Cu^{2+}/H_2O_2 increased the removal efficiency, and on the other hand, the negative role of the Cu/nFe_3O_4 interaction caused it to fall. As presented in Figure 9, increasing the $CuSO_4$ concentration in the presence of the minimum concentration of nFe_3O_4 could raise the removal efficiency due to Fe^{2+} generation that resulted from the $CuSO_4$/nZVI interaction. But the high concentration of $CuSO_4$ with the maximum nFe_3O_4 drops the removal efficiency due to Fe^{2+} consumption resulting from the $CuSO_4/nFe_3O_4$ interaction. The results of the experiments showed that the presence of Cu (II) had two opposite effects on removal efficiency. On the one hand, the positive role of the interaction of Cu^{2+}/nZVI and Cu^{2+}/H_2O_2 increased the removal efficiency, and on the other hand, the negative role of the Cu/nFe_3O_4 interaction caused it to fall. As presented in Figure 9, increasing the $CuSO_4$ concentration in the presence of the minimum concentration of nFe_3O_4 could raise the removal efficiency due to Fe^{2+} generation that resulted from the $CuSO_4$/nZVI interaction. But the high concentration of $CuSO_4$ with the maximum nFe_3O_4 drops the removal efficiency due to Fe^{2+} consumption resulting from the $CuSO_4/nFe_3O_4$ interaction.

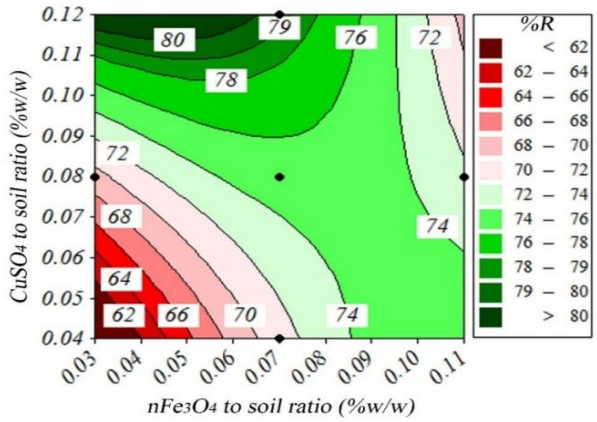

Fig. 9. Counter plot of *tert*-butyl mercaptan removal efficiency as a function of interaction between $CuSO_4$ and nFe_3O_4 with constant amounts of the other main parameters at the center point, T_0=24 °C, pH_0=6.6, Time=20 min.

3.4. Determination of optimal condition for tert-butyl mercaptan removal efficiency

The prediction models showed that the maximum removal efficiency was 99.06% for CCD at the optimum condition in the studied intervals. The optimum condition which is listed in Table 7 suggests that the concentration of H_2O_2, nZVI, and nFe_3O_4 must be at a certain level in the presence of the maximum $CuSO_4$ and minimum initial gasoline concentration in the studied intervals. A verification experiment was conducted to verify the resulting optimized condition. The result showed that the maximum removal efficiency of *tert*-butyl mercaptan from the polluted soil was 99.27% according to the optimum condition. This efficiency was more than some methods like sonication and the modified Fenton process for *tert*-butyl mercaptan remediation from polluted soil [28].

Table 7. Optimal values of the main independent factors for the maximum removal efficiency (%).

$[H_2O_2]_0$ (%W/V)	$(nZVI:S)_0$ (%W/W)	$(nFe_3O_4:S)_0$ (%W/W)	$(I.C:S)_0$ (%W/W)	$(CuSO_4:S)_0$ (%W/W)	Removal efficiency (%R)	
					predicted	Observed
8.9200	0.1194	0.0898	2.5000	0.1200	99.06	99.27

In the results of this study, the maximum *tert*-butyl mercaptan removal efficiency (99.27%) was greater than those of the modified Fenton process (94.14%) [26], the combination of the Fenton with $KMnO_4$ and NaClO (95.71%) [27], and the sonication process (82.83%) [28] in the limited time interval. The nearly complete remediation of *tert*-butyl mercaptan was reported using the sono-Fenton process with the contaminant load of 25000 ppm [29], but it consumed much more energy for sonication compared with the bimetallic modified Fenton process in the present work.

4. Conclusions

Tert-butyl mercaptan is an organosulfur material and its remediation from soil is important to study. The modeling and optimization of *tert*-butyl mercaptan removal efficiency from polluted soil using a bimetallic-nano-modified Fenton process have not been studied before. Pareto analysis and ANOVA indicated that all investigated factors were effective in removal efficiency. Moreover, the interaction of H_2O_2/nZVI, H_2O_2/nFe_3O_4, H_2O_2/$CuSO_4$, nZVI/nFe_3O_4, and nZVI/$CuSO_4$ have a positive effect on the removal efficiency, while nFe_3O_4/$CuSO_4$ has a negative effect. The maximum *tert*-butyl mercaptan removal efficiency was achieved with the lower levels of initial gasoline concentration, the optimum concentration of H_2O_2, nFe_3O_4, nZVI, and the highest concentration of $CuSO_4$ in the studied interval. Surprisingly, iron catalysts addition mode (catalysts mixing before/after addition to soil) was not an effective factor in the studied interval. The method investigated in this study could be used for increasing the removal efficiency of similar organosulfur because of the positive interaction between the reactants.

References

[1] Suravajala, A., Erickson, L. E., Bhandari, A. (2008). Sorption of tertiary butyl mercaptan to indoor materials in contact with air or water. *Journal of environmental engineering*, *134*(3), 161-168.

[2] Karthikeyan, R., Hutchinson, S. L. L., Erickson, L. E. (2012). Biodegradation of tertiary butyl mercaptan in water. *Journal of bioremediation and biodegradation*, *3*(6), DOI: 10.4172/2155-6199.1000156.

[3] Gan, S., Ng, H. K. (2012). Current status and prospects of Fenton oxidation for the decontamination of persistent organic pollutants (POPs) in soils. *Chemical engineering journal*, *213*, 295-317.

[4] Manzano, M. A., Perales, J. A., Sales, D., Quiroga, J. M. (2004). Catalyzed hydrogen peroxide treatment of polychlorinated biphenyl contaminated sandy soils. *Water, air, and soil pollution*, *154*(1-4), 57-69.

[5] Yeh, C. K. J., Hsu, C. Y., Chiu, C. H., Huang, K. L. (2008). Reaction efficiencies and rate constants for the goethite-catalyzed Fenton-like reaction of NAPL-form aromatic hydrocarbons and chloroethylenes. *Journal of hazardous materials*, *151*(2-3), 562-569.

[6] Gan, S., Ng, H. K. (2012). Modified Fenton oxidation of polycyclic aromatic hydrocarbon (PAH)-contaminated soils and the potential of bioremediation as post-treatment. *Science of the total environment*, *419*, 240-249.

[7] Watts, R. J., Haller, D. R., Jones, A. P., Teel, A. L. (2000). A foundation for the risk-based treatment of gasoline-contaminated soils using modified Fenton's reactions. *Journal of hazardous materials*, *76*(1), 73-89.

[8] Chang, M. C., Shu, H. Y., Hsieh, W. P., Wang, M. C. (2007). Remediation of soil contaminated with pyrene using ground nanoscale zero-valent iron. *Journal of the air annd waste management association*, *57*(2), 221-227.

[9] Sun, S. P., Lemley, A. T. (2011). p-Nitrophenol degradation by a heterogeneous Fenton-like reaction on nano-magnetite: process optimization, kinetics, and degradation pathways. *Journal of molecular catalysis A: chemical*, *349*(1-2), 71-79.

[10] Xue, X., Hanna, K., Despas, C., Wu, F., Deng, N. (2009). Effect of chelating agent on the oxidation rate of PCP in the magnetite/H_2O_2 system at neutral pH. *Journal of molecular catalysis A: chemical*, *311*(1-2), 29-35.

[11] Papić, S., Mužic, M., Koprivanac, N., Peternel, I., Deanović, M. (2010). Decolorization of the anthraquinone dye CI reactive Blue 2 by Fenton Oxidation; Statistical Experimental design. *Chemical and biochemical engineering quarterly*, *24*(1), 9-16.

[12] Gan, S., Ng, H. K. (2012). Inorganic chelated modified-Fenton treatment of polycyclic aromatic hydrocarbon (PAH)-contaminated soils. *Chemical engineering journal*, *180*, 1-8.

[13] van Bergen, L. A., Roos, G., De Proft, F. (2014). From thiol to sulfonic acid: Modeling the oxidation pathway of protein thiols by hydrogen peroxide. *The journal of physical chemistry A*, *118*(31), 6078-6084.

[14] Watts, R. J., Teel, A. L. (2005). Chemistry of modified Fenton's reagent (catalyzed H_2O_2 propagations–CHP) for in situ soil and groundwater remediation. *Journal of environmental engineering*, *131*(4), 612-622.

[15] Qin, Y., Luo, S., Geng, S., Jiao, W., Liu, Y. (2018). Degradation and mineralization of aniline by O_3/Fenton process enhanced using high-gravity technology. *Chinese journal of chemical engineering*, *26*(7), 1444-1450.

[16] Kumoro, A. C., Ratnawati, R., Retnowati, D. S. (2015). A simplified kinetics model of natural and iron complex catalysed hydrogen peroxide oxidation of starch. *Asia-Pacific journal of chemical engineering*, *10*(5), 648-658.

[17] Bissey, L. L., Smith, J. L., Watts, R. J. (2006). Soil organic matter–hydrogen peroxide dynamics in the treatment of contaminated soils and groundwater using catalyzed H_2O_2 propagations (modified Fenton's reagent). *Water research*, *40*(13), 2477-2484.

[18] Arslan, A., Öztürk, B. (2009). Applicability of Fenton and photo-Fenton Processes to Combined Industrial and Domestic Wastewater. *Chemical and biochemical engineering quarterly*, *23*(3), 317-322.

[19] Kanel, S. R., Neppolian, B., Choi, H., Yang, J. W. (2003). Heterogeneous catalytic oxidation of phenanthrene by hydrogen peroxide in soil slurry: Kinetics, mechanism, and implication. *Soil and sediment contamination*, *12*(1), 101-117.

[20] Vicente, F., Rosas, J. M., Santos, A., Romero, A. (2011). Improvement soil remediation by using stabilizers and chelating agents in a Fenton-like process. *Chemical engineering journal*, *172*(2-3), 689-697.

[21] Lu, M., Zhang, Z., Qiao, W., Guan, Y., Xiao, M., Peng, C. (2010). Removal of residual contaminants in petroleum-contaminated soil by Fenton-like oxidation. *Journal of hazardous materials*, *179*(1-3), 604-611.

[22] Pereira, M. C., Oliveira, L. C. A., Murad, E. (2012). Iron oxide catalysts: Fenton and Fentonlike reactions–a review. *Clay minerals*, *47*(3), 285-302

[23] Sun, S. P., Lemley, A. T. (2011). p-Nitrophenol degradation by a heterogeneous Fenton-like reaction on nano-magnetite: process optimization, kinetics, and degradation pathways. *Journal of molecular catalysis A: chemical*, *349*(1-2), 71-79.

[24] Zhang, S., Zhao, X., Niu, H., Shi, Y., Cai, Y., Jiang, G. (2009). Superparamagnetic Fe_3O_4 nanoparticles as catalysts for the catalytic oxidation of phenolic and aniline compounds. *Journal of hazardous materials*, *167*(1-3), 560-566.

[25] Jorfi, S., Alavi, S., Jaafarzadeh, N., Ghanbari, F., Ahmadi, M. (2018). COD Removal from High Salinity Petrochemical Wastewater Using Photo-assisted Peroxi-coagulation. *Chemical and biochemical engineering quarterly*, *32*(2), 229-238.

[26] Roohi, P., Fatehifar, E., Alizadeh, R. (2017). Modeling and optimization of fast degradation of contaminated soil with 2-methylpropane-2-thiol by modified Fenton process. *Modares civil engineering journal*, *17*(4), 77-88.

[27] Roohi, P., Fatehifar, E., Alizadeh, R. (2016). Rapid degradation of contaminated soil with 2-methylpropane-2-thiol by H2O2/KMnO4/NaClO system: process modeling and optimization. *Asia-pacific journal of chemical engineering*, *11*(5), 743-756.

[28] Roohi, P., Fatehifar, E., Alizadeh, R. (2016). Mathematical modeling and optimization of sonication remediation of soil polluted with 2-methylpropane-2-thiol. *Advances in environmental technology*, *1*, 137-146.

[29] Rouhi, P. (2019). Efficient Rapid Deodorization of Mercaptan-Contaminated Soil by Sono-Fenton Process: Response surface modeling and optimization. *Physical chemistry research*, *7*(1), 53-64.

[30] Kalainesan, S., Erickson, L. E., Hutchinson, S. L. L., Urban, J. E., & Karthikeyan, R. (2006). Transformation of tertiary butyl mercaptan in aerobic environments. *Environmental progress*, *25*(3), 189-200.

[31] Danish, M., Gu, X., Lu, S., Naqvi, M. (2016). Degradation of chlorinated organic solvents in aqueous percarbonate system using zeolite supported nano zero valent iron (Z-nZVI) composite. *Environmental science and pollution research*, *23*(13), 13298-13307.

[32] Mukherjee, R., Kumar, R., Sinha, A., Lama, Y., Saha, A. K. (2016). A review on synthesis, characterization, and applications of nano zero valent iron (nZVI) for

environmental remediation. *Critical reviews in environmental science and technology*, *46*(5), 443-466.

[33] Ezzatahmadi, N., Ayoko, G. A., Millar, G. J., Speight, R., Yan, C., Li, J., Xi, Y. (2017). Clay-supported nanoscale zero-valent iron composite materials for the remediation of contaminated aqueous solutions: a review. *Chemical engineering journal*, *312*, 336-350.

[34] Wei, H., Hu, D., Su, J., Li, K. (2015). Intensification of levofloxacin sono-degradation in a US/H_2O_2 system with Fe_3O_4 magnetic nanoparticles. *Chinese journal of chemical engineering*, *23*(1), 296-302.

[35] Li, Y., Jin, Z., Li, T., Li, S. (2011). Removal of hexavalent chromium in soil and groundwater by supported nano zero-valent iron on silica fume. *Water science and technology*, *63*(12), 2781-2787.

[36] Fu, F., Dionysiou, D. D., Liu, H. (2014). The use of zero-valent iron for groundwater remediation and wastewater treatment: a review. *Journal of hazardous materials*, *267*, 194-205.

[37] Choi, K., Lee, W. (2012). Enhanced degradation of trichloroethylene in nano-scale zero-valent iron Fenton system with Cu (II). *Journal of hazardous materials*, *211*, 146-153.

[38] Diao, Z. H., Xu, X. R., Chen, H., Jiang, D., Yang, Y. X., Kong, L. J Liu, L. (2016). Simultaneous removal of Cr (VI) and phenol by persulfate activated with bentonite-supported nanoscale zero-valent iron: reactivity and mechanism. *Journal of hazardous materials*, *316*, 186-193.

[39] Stumm, W. (1995). The inner-sphere surface complex-a key to understanding surface reactivity. *Aquatic chemistry*, Chapter 2, pp. 1-32.

[40] Sparks, D. L. (2003). *Environmental soil chemistry*. Elsevier.

[41] Sheini, F. J., Singh, J., Srivasatva, O. N., Joag, D. S., More, M. A. (2010). Electrochemical synthesis of Cu/ZnO nanocomposite films and their efficient field emission behaviour. *Applied surface science*, *256*(7), 2110-2114.

[42] Wu, H., Wang, L. S. (1997). A study of nickel monoxide (NiO), nickel dioxide (ONiO), and Ni (O_2) complex by anion photoelectron spectroscopy. *The journal of chemical physics*, *107*(1), 16-21.

[43] Zhou, H., Kang, L., Zhou, M., Zhong, Z., Xing, W. (2018). Membrane enhanced COD degradation of pulp wastewater using Cu_2O/H_2O_2 heterogeneous Fenton process. *Chinese journal of chemical engineering*, *26*(9), 1896-1903.

[44] Xia, M., Long, M., Yang, Y., Chen, C., Cai, W., Zhou, B. (2011). A highly active bimetallic oxides catalyst supported on Al-containing MCM-41 for Fenton oxidation of phenol solution. *Applied catalysis B: environmental*, *110*, 118-125.

[45] Liu, Xinwen, Zhengxian Chen, Zuliang Chen, Mallavarapu Megharaj, and Ravendra Naidu. "Remediation of Direct Black G in wastewater using kaolin-supported bimetallic Fe/Ni nanoparticles." *Chemical engineering journal,* 223 (2013): 764-771.

[46] Karthikeyan, S., Pachamuthu, M. P., Isaacs, M. A., Kumar, S., Lee, A. F., Sekaran, G. (2016). Cu and Fe oxides dispersed on SBA-15: A Fenton type bimetallic catalyst for N, N-diethyl-p-phenyl diamine degradation. *Applied catalysis B: Environmental*, *199*, 323-330.

[47] Gong, J., Lee, C. S., Kim, E. J., Chang, Y. Y., Chang, Y. S. (2016). Enhancing the reactivity of bimetallic Bi/Fe0 by citric acid for remediation of polluted water. *Journal of hazardous materials*, *310*, 135-142.

[48] Zandsalimi, Y., Taymori, P., Darvishi Cheshmeh Soltani, R., Rezaee, R., Abdullahi, N., Safari, M. (2015). Photocatalytic removal of Acid Red 88 dye using zinc oxide nanoparticles fixed on glass plates. *Journal of advances in environmental health research*, *3*(2), 102-110.

[49] Grčić, I., Vujević, D., Koprivanac, N. (2010). Statistical evaluation of UV/TiO_2/H_2o_2 and fe2+/H_2o_2 process for the treatment of coloured wastewater; a comparative study. *Chemical and biochemical engineering quarterly*, *24*(4), 387-400.

[50] Smidt, M., Kusic, H., Juretic, D., Novak Stankov, M., Ukic, S., Bolanca, T., Loncaric Bozic, A. (2015). Modeling photo-oxidative degradation of aromatics in water. Optimization study using response surface and structural relationship approaches. *Industrial and engineering chemistry research*, *54*(20), 5427-5441.

[51] Prabhakaran, D., Kannadasan, T., Thirumarimurugan, M., Chellamboli, C. (2012). Experimental studies on electrochemical and photo oxidation of effluent containing Ethyl Benzene and optimization Using RSM. *International journal of bioscience, biochemistry and bioinformatics*, *2*(6), 369.

[52] Mokhtarani, N., Yasrobi, S. Y., Ganjidoust, H. (2015). Optimization of ozonation process for a composting leachate-contaminated soils treatment using response surface method. *Ozone: Science and engineering*, *37*(3), 279-286.

[53] Hazime, R., Nguyen, Q. H., Ferronato, C., Huynh, T. K. X., Jaber, F., Chovelon, J. M. (2013). Optimization of imazalil removal in the system UV/TiO_2/$K_2S_2O_8$ using a response surface methodology (RSM). *Applied catalysis B: environmental*, *132*, 519-526.

[54] Long, A., Zhang, H., Lei, Y. (2013). Surfactant flushing remediation of toluene contaminated soil: Optimization with response surface methodology and surfactant recovery by selective oxidation with sulfate radicals. *Separation and purification technology*, *118*, 612-619.

[55] Kalantary, R. R., Badkoubi, A., Mohseni-Bandpi, A., Esrafili, A., Jorfi, S., Dehghanifard, E., Baneshi, M. M. (2013). Modification of PAHs biodegradation with

humic compounds. *Soil and sediment contamination: An international journal*, *22*(2), 185-198.

[56] Estebar, M., Amin, M. M., Poursafa, P., Ghasemian, M., Jaafarzadeh, N., Hashemi, H., Fatehizadeh, A. (2012). Biodegradation of benzene-toluene-xylene in petrochemical industries wastewater through anaerobic sequencing biofilm batch reactor in bench scale. *International journal of environmental health engineering*, *1*(1), 22.

[57] Jackson, M. L., Lim, C. H., Zelazny, L. W. (1986). Oxides, Hydroxides, and Aluminosilicates 1. *Methods of soil analysis: Part 1—physical and mineralogical methods*, (methodsofsoilan1), 101-150.

[58] Nelson, D. W., & Sommers, L. E. (1996). Total carbon, organic carbon, and organic matter. *Methods of soil analysis part 3—chemical methods*, (methodsofsoilan3), 961-1010.

[59] Wei, T. K., Manickam, S. (2012). Response Surface Methodology, an effective strategy in the optimization of the generation of curcumin-loaded micelles. *Asia-Pacific journal of chemical engineering*, *7*, S125-S133.

[60] Aghaeinejad-Meybodi, A., Ebadi, A., Shafiei, S., Khataee, A., Rostampour, M. (2015). Degradation of antidepressant drug fluoxetine in aqueous media by ozone/H_2O_2 system: process optimization using central composite design. *Environmental technology*, *36*(12), 1477-1488.

[61] Ahmadi, R., Khodadadi Darban, A. (2013). Modeling and optimization of nano-bubble generation process using response surface methodology. *International journal of nanoscience and nanotechnology*, *9*(3), 151-162.

[62] Kahforoushan, D., Bezaatpour, J., Fatehifar, E. (2014). Effect of various parameters on emission factors of gas flares. *Iranian journal of chemical engineering*, *11*(3), 59-66.

[63] Hosseini, M., Khoshfetrat, A. B., Sahraei, E., Ebrahimi, S. (2014). Continuous nitrifying granular sludge bioreactor: influence of aeration and ammonium loading rate. *Process safety and environmental protection*, *92*(6), 869-878.

[64] Dehghani, M., Nasseri, S., Hashemi, H. (2013). Study of the bioremediation of atrazine under variable carbon and nitrogen sources by mixed bacterial consortium isolated from corn field soil in Fars Province of Iran. *Journal of environmental and public health*, *2013*. 1-7.

[65] Aghaeinejad-Meybodi, A., Ebadi, A., Shafiei, S., Khataee, A. R., Rostampour, M. (2015). Modeling and optimization of antidepressant drug fluoxetine removal in aqueous media by ozone/H2O2 process: comparison of central composite design and artificial neural network approaches. *Journal of the Taiwan institute of chemical engineers*, *48*, 40-48.

[66] Hadavifar, M., Zinatizadeh, A. A., Younesi, H., Galehdar, M. (2010). Fenton and photo-Fenton treatment of distillery effluent and optimization of treatment conditions with response surface methodology. *Asia-Pacific Journal of chemical engineering*, *5*(3), 454-464.

[67] Karimi, A., Mahdizadeh, F., Salari, D., Vahabzadeh, F., Khataee, A. (2012). Enzymatic scavenging of oxygen dissolved in water: Application of response surface methodology in optimization of conditions. *Chemical industry and chemical Eengineering quarterly/CICEQ*, *18*(3), 431-439.

[68] Su, C., Puls, R. W. (2004). Nitrate reduction by zerovalent iron: effects of formate, oxalate, citrate, chloride, sulfate, borate, and phosphate. *Environmental science and technology*, *38*(9), 2715-2720.

[69] Furman, O., Laine, D. F., Blumenfeld, A., Teel, A. L., Shimizu, K., Cheng, I. F., Watts, R. J. (2009). Enhanced reactivity of superoxide in water− solid matrices. *Environmental science and technology*, *43*(5), 1528-1533.

[70] Pignatello, J. J., Oliveros, E., MacKay, A. (2006). Advanced oxidation processes for organic contaminant destruction based on the Fenton reaction and related chemistry. *Critical reviews in environmental science and technology*, *36*(1), 1-84.

[71] Baciocchi, R. (2013). Principles, developments and design criteria of in situ chemical oxidation. *Water, air, and soil pollution*, *224*(12), 1-11.

[72] Jorfi, S., Rezaee, A., Moheb-ali, G. A., alah Jaafarzadeh, N. (2013). Pyrene removal from contaminated soils by modified Fenton oxidation using iron nano particles. *Journal of environmental health science and engineering*, *11*(1), 17-25.

[73] Yan, N., Liu, F., Huang, W. (2013). Interaction of oxidants in siderite catalyzed hydrogen peroxide and persulfate system using trichloroethylene as a target contaminant. *Chemical engineering journal*, *219*, 149-154.

[74] Xu, J., Tang, J., Baig, S. A., Lv, X., Xu, X. (2013). Enhanced dechlorination of 2, 4-dichlorophenol by Pd/$FeFe_3O_4$ nanocomposites. *Journal of hazardous materials*, *244*, 628-636.

[75] Üzüm, Ç., Shahwan, T., Eroğlu, A. E., Hallam, K. R., Scott, T. B., Lieberwirth, I. (2009). Synthesis and characterization of kaolinite-supported zero-valent iron nanoparticles and their application for the removal of aqueous Cu2+ and Co^{2+} ions. *Applied clay science*, *43*(2), 172-181.

[76] Benarji, P.T., and Raju, K. (2011). Reductimetric determination of Copper (II) with Iron (ii) in Phosphoric Acid medium and in presence of Bromide ion. *Research journal of chemical sciences*, *1*, 2.

[77] LiA, F., ZhouA, S., ZhuangA, L., TaoA, L., LiA, X., WuA, C., LiuA, T. (2010). Biogeochemical interactions between Fe (II)/(III) species cycles and transformation of

reducible substrates in subtropical soils. In *19th world congress of soil science*.

[78] Stumm, W., Lee, G. F. (1961). Oxygenation of ferrous iron. *Industrial engineering chemistry*, *53*(2), 143-146.

[79] Matocha, C. J., Karathanasis, A. D., Rakshit, S., Wagner, K. M. (2005). Reduction of copper (II) by iron (II). *Journal of environmental quality*, *34*(5), 1539-1546.

[80] He, J., Yang, X., Men, B., Wang, D. (2016). Interfacial mechanisms of heterogeneous Fenton reactions catalyzed by iron-based materials: A review. *Journal of environmental sciences*, *39*, 97-109.

[81] Lee, H., Lee, H. J., Sedlak, D. L., Lee, C. (2013). pH-Dependent reactivity of oxidants formed by iron and copper-catalyzed decomposition of hydrogen peroxide. *Chemosphere*, *92*(6), 652-658.

[82] Huling, S. G., & Pivetz, B. E. (2006). In-situ chemical oxidation (No. EPA/600/R-06/072). Environmental Protection Agency Washington DC Office Of Water.